catalysts

MDPI

Article

Effect of Copper Precursors on the Activity and Hydrothermal Stability of Cu^{II}–SSZ–13 NH_3–SCR Catalysts

Meixin Wang [1], Zhaoliang Peng [1], Changming Zhang [1], Mengmeng Liu [1], Lina Han [2], Yaqin Hou [3], Zhanggen Huang [3], Jiancheng Wang [1,*], Weiren Bao [1] and Liping Chang [1]

1 Key Laboratory of Coal Science and Technology, Ministry of Education and Shanxi Province, Taiyuan University of Technology, Taiyuan 030024, China; wangmeixinabc@yeah.net (M.W.); pengzhaoliang@tyut.edu.cn (Z.P.); zhangchangming@tyut.edu.cn (C.Z.); liumengmeng@tyut.edu.cn (M.L.); baoweiren@tyut.edu.cn (W.B.); lpchang@tyut.edu.cn (L.C.)

2 College of Materials Science and Engineering, Taiyuan University of Technology, Taiyuan 030024, China; hanlina@tyut.edu.cn

3 State Key Laboratory of Coal Conversion, Institute of Coal Chemistry, Chinese Academy of Sciences, Taiyuan 030001, China; houyaqin@sxicc.ac.cn (Y.H.); zghuang@sxicc.ac.cn (Z.H.)

* Correspondence: wangjiancheng@tyut.edu.cn; Tel.: +86-138-3462-9730

Received: 29 August 2019; Accepted: 17 September 2019; Published: 19 September 2019

Abstract: A series of Cu^{II}–SSZ–13 catalysts are prepared by in-situ hydrothermal method using different copper precursors ($Cu^{II}(NO_3)_2$, $Cu^{II}SO_4$, $Cu^{II}Cl_2$) for selective catalytic reduction of NO by NH_3 in a simulated diesel vehicle exhaust. The catalysts were characterized by X–ray diffraction (XRD), scanning electron microscope (SEM), X–ray photoelectron spectroscopy (XPS), N_2 adsorption-desorption, hydrogen-temperature-programmed reduction (H_2–TPR), ammonia temperature-programmed desorption (NH_3–TPD), and ^{27}Al and ^{29}Si solid state Nuclear Magnetic Resonance (NMR). The Cu^{II}–SSZ–13 catalyst prepared by $Cu^{II}(NO_3)_2$ shows excellent catalytic activity and hydrothermal stability. The NO conversion of Cu^{II}–SSZ–13 catalyst prepared by $Cu^{II}(NO_3)_2$ reaches 90% at 180 °C and can remain above 90% at a wide temperature range of 180–700 °C. After aging treatment at 800 °C for 20 h, the Cu^{II}–SSZ–13 catalyst prepared by $Cu^{II}(NO_3)_2$ still exhibits above 90% NO conversion under a temperature range of 240–600 °C. The distribution of Cu species and the Si/Al ratios in the framework of the synthesized Cu^{II}–SSZ–13 catalysts, which determine the catalytic activity and the hydrothermal stability of the catalysts, are dependent on the adsorption capacity of anions to the cation during the crystallization process due to the so called Hofmeister anion effects, the NO_3^- ion has the strongest adsorption capacity among the three kinds of anions (NO_3^-, Cl^-, and SO_4^{2-}), followed by Cl^- and SO_4^{2-} ions. Therefore, the Cu^{II}–SSZ–13 catalyst prepared by $Cu^{II}(NO_3)_2$ possess the best catalytic ability and hydrothermal stability.

Keywords: selective catalytic reduction; Cu^{II}–SSZ–13; copper precursor; hydrothermal stability; emission control of diesel engine exhaust

1. Introduction

The emission of nitrogen oxides is a major cause of unhealthy air quality and is strictly regulated in many places. To meet regulations, controlling the emission of nitrogen oxides from diesel exhaust is one important topic in catalysis [1,2]. The selective catalytic reduction of NO_x by ammonia (NH_3-SCR) is one of the most effective approaches to convert NO_x due to its high fuel economy, and high denitrification efficiency [3,4]. The core issue of this technology is the development of environmentally friendly SCR catalysts with high activity, wide operating temperature window, and excellent hydrothermal stability.

Prior to the application of molecular sieve catalysts, NO_x abatement technology relied primarily on V_2O_5-WO_3/TiO_2 as a NO_x removal catalyst [5,6]. In recent years, the Cu^{II}−SSZ−13 molecular sieve used as NH_3-SCR catalysts has become a hot topic due to its wide temperature window, high N_2 selectivity, and excellent hydrothermal stability [7–9]. In addition, Cu^{II}−SSZ−13 shows its superiority in hydrothermal stability under moderate aging temperatures (e.g., 750–800 °C) compared to other well-known Cu molecular sieves (e.g., Cu-ZSM-5, Cu-beta, and Cu-Y) [10].

Recently, the Cu^{II}−SSZ−13 catalysts are usually synthesized by hydrothermal method and subsequent ion exchange process. Han et al. [11] prepared Cu^{II}−SSZ−13 catalyst using N, N, N-trimethyl-1-adamantane ammonium hydroxide (TMAda-OH) as template by microwave, dynamic and static hydrothermal methods, respectively. Shishkiny et al. [12] synthesized functionalized Cu^{II}−SSZ−13 catalyst by introducing Cu and Fe ions into the Na-SSZ-13 catalyst during the ion exchange process. The industrial application of SSZ-13 molecular sieve catalyst is limited due to the high costs of TMAda-OH template. Ren et al. [13] developed an in situ method to synthesize Cu^{II}−SSZ−13 using low-cost copper teraethylenepentamine (Cu-TEPA) as template, which reduced economic cost the Cu^{II}−SSZ−13 catalyst. Zhang et al. [14] compared Cu^{II}−SSZ−13 catalysts prepared by ion-exchange (Cu^{II}−SSZ−13−I) and in-situ synthesis methods (Cu^{II}−SSZ−13−O), and found that Cu^{II}−SSZ−13−O showed higher $DeNO_x$ activity and stronger Lewis acid site strengths than Cu^{II}−SSZ−13−I. Cu^{II}−SSZ−13 was prepared by selecting a novel low-temperature solid-state ion-exchange (LT−SSIE) method using $Cu^{II}Ac_2$ and $Cu^{II}(NO_3)_2$ as Cu precursors, showing comparable SCR activity and hydrothermal stability to the traditional solution ion-exchanged Cu^{II}−SSZ−13 with a similar Cu loading [15]. Paolucci et al. [16] have worked out a scenario that is based on the formation of the Cu−ammonia complex $Cu(NH_3)_2^+$ mechanism shows that the actual active sites for NO_x reduction are not static structures but dynamic and come and go as the reaction proceeds. Borfecchia et al. [17] provide a comprehensive overview on the structural complexity of Cu−CHA materials, it has been shown that the active site in the low temperature NH_3−SCR catalyst is a mobile Cu-molecular entity that "lives in symbiosis" with an inorganic solid framework. Only in the high temperature NH_3−SCR regime do the mobile Cu species lose their ligands and find docking sites at the internal walls of the molecular sieve framework. Marberger et al. [18] monitored the evolution of various Cu species in Cu^{II}−SSZ−13 and experimentally identified crucial characteristics of the SCR catalyst in the low-temperature regime: the rate-limiting re-oxidation of $Cu^{I}(NH_3)_2$ is strongly influenced by NH_3 inhibition; the active $Cu^{II}(NH_3)_4$ species are mainly formed below 250 °C; and the modification of the active sites with increasing temperatures is driven by the loss of NH_3 coordinating Cu species.

It should be noted that the synthesis of molecular sieves via hydrothermal method is a multi-variable process. The crystallization temperature, duration, dynamic/static, as well as the prescriptions of anions and cations have important influences on the physicochemical properties of the final molecular sieve products, which further determine the performances of the catalysts. In the process of in-situ synthesis of Cu^{II}−SSZ−13 catalyst, the distribution of metal cations on the molecular sieve framework determines its structure properties and catalytic performance. The metal cations can affect the aggregation state, condensation rate, and colloidal state of silicate materials in the formation in the reaction system [19]. The anions also have influences on the synthesis of silicon-alumina molecular sieves. It has been reported that the crystallization time of ZSM−5 and TS−1 can be regulated by the oxyacid anion [20]. In the early days, Hofmeister studied the ability of different salt solutions to denature proteins, and called the relative effectiveness of anions to produce different specificities on a wide range of phenomena the Hofmeister anion effect [21]. Alexander V [22] investigated a series of Hofmeister anions that may be arranged in the following sequence: $SO_4^{2-} > Cl^- \sim NO_3^-$ with decreasing zeolite Beta formation potency from left to right. The Hofmeister anion effect can influence the surface activity of the mesoporous materials. The adsorption ability of anion to the cation: $NO_3^- > Cl^- > SO_4^{2-}$ [23,24]. Anion species will change hydrolysis rate of silicate liquid precursor and the size of template agent micelle, which finally results in the differences of the surface properties and the morphology of molecular sieve catalyst after calcination. In short, the anion

can change hydrolysis rate of precursor and the structure of colloid formed by the template agent, which affects the framework structure, crystal structure, morphology, and the catalytic properties of the final Cu^{II}–SSZ–13 molecular sieve.

In this work, Cu^{II}–SSZ–13 catalysts were prepared by in-situ hydrothermal synthesis method for NO selective catalytic reduction with NH_3 in simulated diesel vehicles exhaust. Three kinds of copper precursors ($Cu^{II}(NO_3)_2$, $Cu^{II}SO_4$, $Cu^{II}Cl_2$) were used to investigate the effect of anions on the structure, catalytic activity, and hydrothermal stability of Cu^{II}–SSZ–13 catalysts. The NO conversion, N_2 selectivity, and the structure characterization of the fresh and aged Cu^{II}–SSZ–13 catalysts were investigated in detail.

2. Results and Discussion

2.1. Catalytic Activity

Figure 1 shows the conversion of NO, N_2 selectivity, and N_2O yield of fresh and aged Cu^{II}–SSZ–13 catalysts. As shown in Figure 1a, the Cu^{II}–SSZ–13 catalysts prepared by three kinds of copper precursors all exhibit excellent catalytic activity. Compared with the other samples, the NO conversion of the F–NO_3 sample reaches 90% at 180 °C and has a widest temperature window (180–700 °C). The Cu^{II}–SSZ–13 catalysts prepared by three kinds of copper precursors declines dramatically after aging at 800 °C for 20 h as shown in Figure 1b. However, the NO conversion of the A–NO_3 sample exceeds 90% ranging from 140 to 620 °C and just declines a little at the temperature range of 240–600 °C.

Figure 1c,d shows that the ammonia oxidation ability of the fresh and aged Cu^{II}–SSZ–13 catalysts is almost the same over below 300 °C. The stoichiometric relationship between ammonia and NO_x conversion is 1:1 indicating that standard SCR occurs at this temperature range. However, at the high temperature range, the ammonia conversion rate is significantly higher than the NO_x conversion rate, indicating that the ammonia oxidation reaction has occurred [25,26].

The three fresh catalysts exhibit 100% N_2 selectivity in the range of 100–200 °C and 440–700 °C as shown in Figure 1d. While, F–NO_3 sample has the lowest N_2O yield (<15 ppm) among the three samples. Moreover, the amounts of N_2O produced in all aged Cu^{II}–SSZ–13 catalysts are obviously decreased after 300 °C (Figure 1e). The A–NO_3 sample has lower N_2O production (<12 ppm), and shows 100% N_2 selectivity in the range of 100–180 °C and 340–700 °C. The high N_2 selectivity of Cu^{II}–SSZ–13 catalysts is affected by the type of molecular sieve structure and ammonia oxidation ability [10,27]. The formation of N_2O is mainly related to NO_x reacting with proton-adsorbed NH_3 in which NH_4NO_3 that forms on protonic sites could slowly decompose [28].

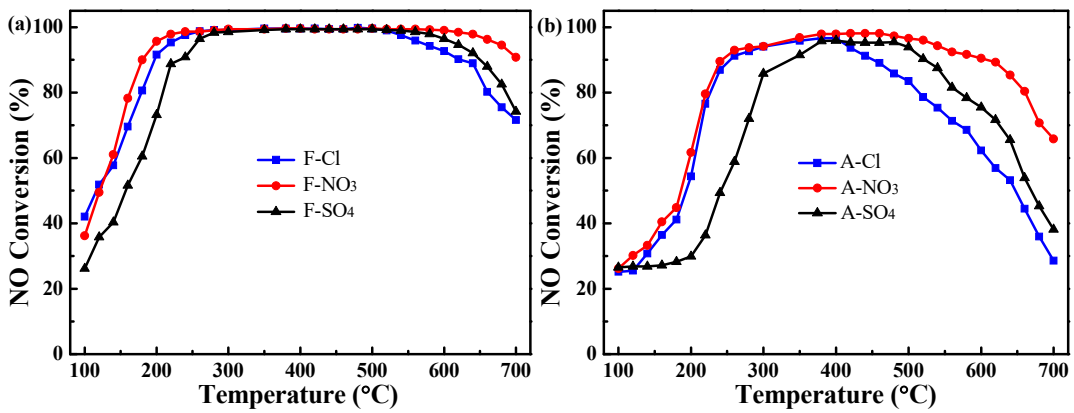

Figure 1. *Cont.*

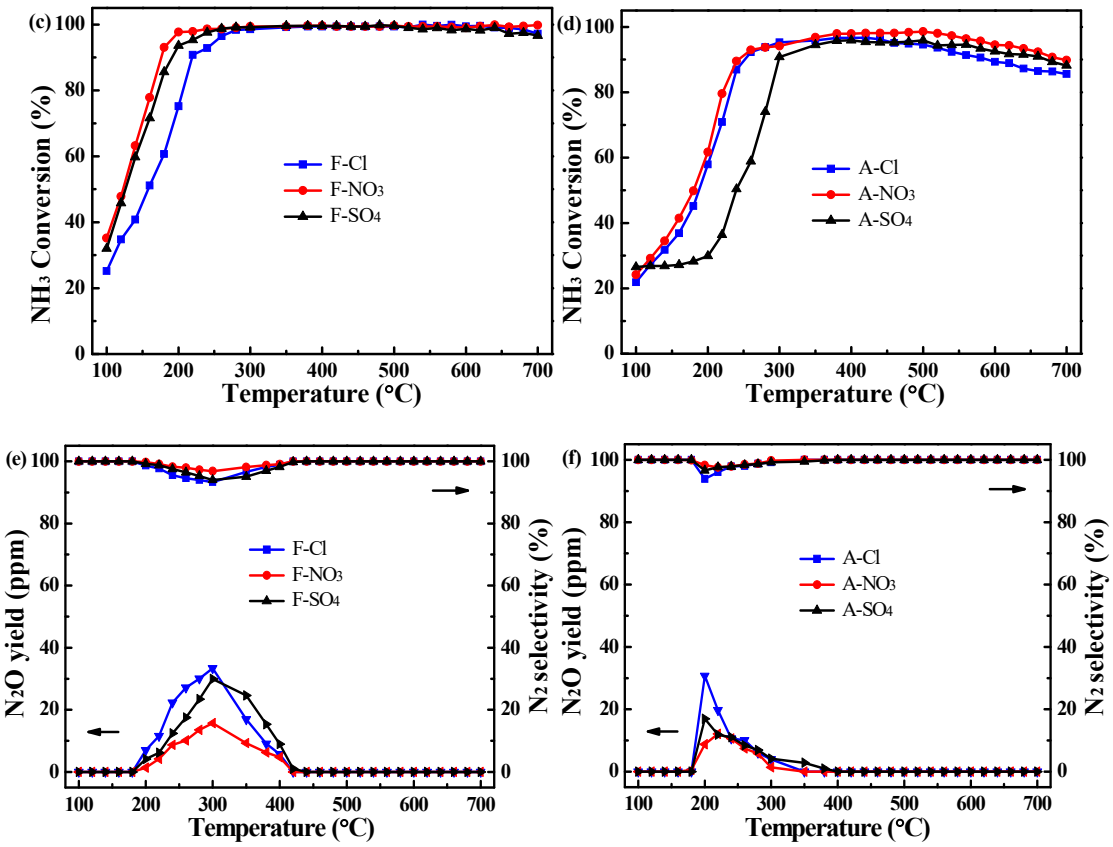

Figure 1. NO conversion (**a**,**b**), NH_3 conversion (**c**,**d**), N_2 selectivity and N_2O yield (**e**,**f**) of Cu^{II}–SSZ–13 catalysts before and after hydrothermal aging treatment. (Feed gas: 0.05% NO, 0.05% NH_3, 5% O_2, 10% H_2O, He balance, gaseous hourly space velocity (GHSV) = 40,000 h^{-1}).

2.2. *Structure and Morphology*

2.2.1. X-ray Diffraction (XRD) Results

The X–ray diffraction (XRD) results of all Cu^{II}–SSZ–13 catalysts are shown in Figure S1. The fresh and aged samples exhibit characteristic diffraction peaks of SSZ-13 at 2θ = 9.5°, 14.0°, 16.1°, 17.8°, 20.7°, 25.0°, 30.7° [2,29,30]. The fresh samples show perfect crystal structure and high crystallinity, among which the peaks of the F–Cl sample is stronger than that of F–NO_3 and F–SO_4 samples (Figure S1a). It can be inferred that the copper precursors can affect the crystallinity and regularity of the fresh samples. No distinct diffraction peaks can be observed for the A–SO_4 sample (Figure S1b), which means that the crystal structure of the A–SO_4 sample is severely destroyed. The Cu^{II}–SSZ–13 prepared by the $Cu^{II}(NO_3)_2$ sample has the smallest change of characteristic peak after aging, which means the hydrothermal stability of these samples are the best. However, there are no diffraction peaks of CuO observed before and after hydrothermal aging. It means that the Cu content is low, or the Cu species are well-dispersed [4].

The grain size parameters with scanning angle near 20° for all Cu^{II}–SSZ–13 catalysts are shown in Table 1. The particle size of F–SO_4 and F–Cl samples are 31.21 and 30.51 nm, respectively, while that of F–NO_3 sample is 27.93 nm. It indicated that F–NO_3 sample has small grains, which may be due to the fact that adsorption capacity of NO_3^- anions on cationic is much larger than those of the SO_4^{2-} and Cl^- anions. NO_3^- ions easily lose water molecules in the process of crystallization or directly utilize water molecules to dissolve other substances on the interface. Its large molecular weight has little effect on surface active agent charge, leading to form small spherical micelles and finally generate small SSZ–13 grain size. The SO_4^{2-} ions frequently lead to a higher surface tension and a salting-out effect (aggregation of cations), which may influence the entering of copper ions to the pores of SSZ–13

and gathering on the support surface [23]. After aging, the diameter size of all the samples reduced. The grain parameters of the sample A−SO_4 was not calculated because there are no obvious diffraction peaks observed over the scanning angle from 5° to 50°. The particle size of the A−NO_3 and A−Cl samples are 23.64 and 27.19 nm, respectively. It shows that the grain size of the A−NO_3 sample is also the smallest. The grain size of the F−Cl sample decreases to a smaller extent after aging, which can be used to explain why the $Cu^{II}(NO_3)_2$ sample has strong anti-aging ability.

Table 1. Grain size parameters of Cu^{II}−SSZ−13 catalysts before and after hydrothermal aging treatment.

Samples	Angle (°)	FWHM	Diameter (nm)	Area (m^2)
F−Cl	20.93	0.26	30.51	3024
A−Cl	20.96	0.29	27.19	1925
F−NO_3	20.69	0.29	27.93	2620
A−NO_3	20.87	0.34	23.64	1761
F−SO_4	20.69	0.26	31.21	2639
A−SO_4	-	-	-	-

2.2.2. N_2 Adsorption Results

In order to investigate the effect of different copper precursors on the pore structure of Cu^{II}−SSZ−13, $Cu^{II}(NO_3)_2$, $Cu^{II}SO_4$ and $Cu^{II}Cl_2$ samples were selected for structural analysis. The results are shown in Table 2. The specific surface areas of F-NO_3 and F−Cl samples are more than 300 m^2/g, while that of F−SO_4. sample is only 233.44 m^2/g. The pore volume and pore size of the F−Nit. sample are 0.13 cm^3/g and 0.65 nm, respectively. After aging, the specific surface area of all samples reduced to varying degrees. The specific surface area and pore volume of the A−SO_4 sample decrease significantly, which is consistent with SSZ−13 peaks disappearance in the XRD. The pore volume and pore size of the A−NO_3 and A−Cl samples are slightly reduced. It indicates that the $Cu^{II}(NO_3)_2$ and $Cu^{II}Cl_2$ samples are beneficial to strengthen the stability of the molecular sieve catalyst framework structure, and improve the anti-aging properties of the catalysts. Moreover, the pore size of the $Cu^{II}(NO_3)_2$ sample before and after aging are the smallest, showing that it has an excellent shape-selective role during the process of gas reaction.

Table 2. Pore structure results of Cu^{II}−SSZ−13 catalysts before and after hydrothermal aging treatment.

Samples	S_{BET} (m^2/g)	V (cm^3/g)	D (nm)
F−Cl	363.99	0.15	0.77
A−Cl	242.15	0.10	0.67
F−NO_3	301.64	0.13	0.65
A−NO_3	145.84	0.08	0.56
F−SO_4	233.44	0.12	1.07
A−SO_4	11.64	0.01	0.49

2.2.3. Scanning Electron Microscope (SEM) Results

Figure 2 shows scanning electron microscope (SEM) pictures of Cu^{II}−SSZ−13 catalysts before and after aging. The grain size of F−SO_4 and F−Cl samples are relatively large and gather together in clusters. However, the F−NO_3 sample presents a neat and angular cubic crystal grain size, large quantity, and good dispersion. Furthermore, the grain sizes of the entire sample are damaged after aging. The A−SO_4 and A−Cl samples have no obvious cubic grain size. The agglomeration phenomenon is very serious. Although the grain size of the $Cu^{II}(NO_3)_2$ sample is slightly damaged, it can still maintain complete cubic shape and relatively uniform distribution.

To sum up, during the process of crystal nucleus growth, the adsorption capacity of different anions on the template micelles is very different due to the effect of Hofmeister anion effects, which has

a direct impact on the formation and growth of crystal grain [23]. It causes the diverse skeletal-structure properties of Cu^{II}−SSZ−13, thereby making the catalyst form different morphologies.

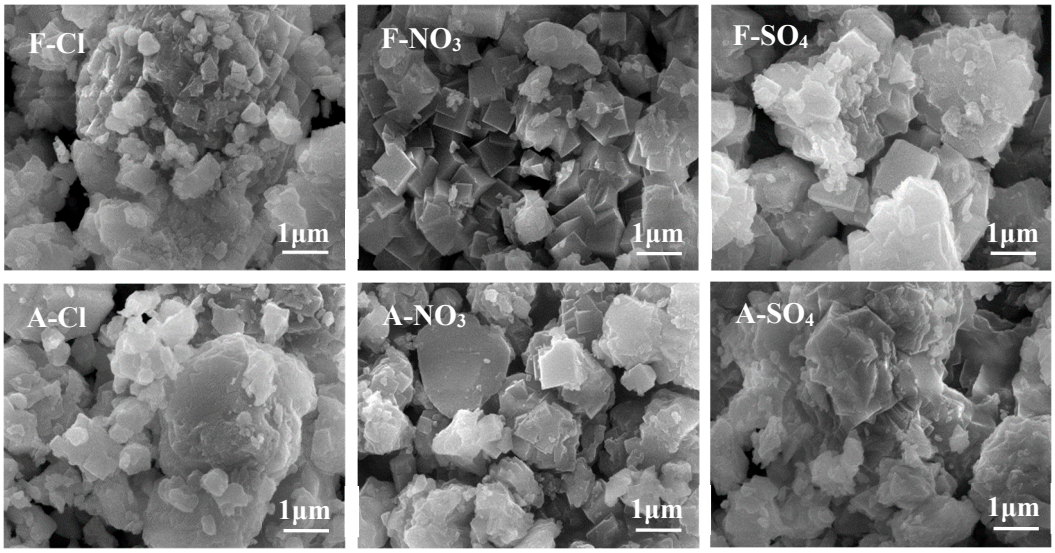

Figure 2. Scanning electron microscope (SEM) images of Cu^{II}−SSZ−13 catalysts before and after hydrothermal aging treatment.

2.2.4. Hydrogen-Temperature-Programmed Reduction (H_2−TPR) Results

The hydrogen-temperature-programmed reduction (H_2−TPR) profiles of Cu^{II}−SSZ−13 catalysts are displayed in Figure 3. It can be seen that the copper precursors have a significant effect on the distribution of Cu species in Cu^{II}−SSZ−13. There are several types of cationic sites in CHA: in [31–33] the H_2 reduction peaks at 180–200 and 200–280 °C stand for the reduction of isolated Cu^{II} ions to Cu^{I} ions in the eight ring and CHA cages, respectively; the H_2 reduction peaks at 280–500 °C are assigned to the reduction of the stable Cu^{II} in double six-rings. The reduction peaks of 500–1000 °C are due to the reduction of Cu^{I} to Cu^{0}. As shown in Figure 3, the H_2−TPR process of isolated Cu^{II} on Cu^{II}−SSZ−13 catalysts are divided into two steps: reduction of Cu^{II}→Cu^{I} at low temperature (<500 °C) and Cu^{I}→Cu^{0} at high temperature (>500 °C) [14]. The fresh samples are shown in Figure 3a, the peak at around 240 °C is assigned to the reduction of isolated Cu^{II}→Cu^{I} in the CHA cage. Different reduction peaks areas appear at 375 °C, indicating the presence of different isolated Cu^{II} ions in the stable six-membered ring. At 500–1000 °C, two different types reduction peaks of Cu^{I} into Cu^{0} appear in three samples, which can be unstable Cu^{I} at low temperature (550 °C) and stable Cu^{I} at high temperature (850 °C) [30,34].

After hydrothermal aging, the aged sample's H_2 reduction peak decrease and move to the higher temperature, indicating the oxidation capacity of Cu species is weakened (Figure 3b). However, the A−NO_3 sample still has significant reduction peaks at 550 and 813 °C. The H_2 reduction peak of at 813 °C represents the reduction of extremely stable Cu^{I} ions. It is worth noting that the reduction temperature of this kind of stable Cu^{I} ion is when the structure of the molecular sieve begins to collapse [30,34]. This is consistent with the XRD results. The A−NO_3 sample has higher stable Cu^{I} content and therefore it can maintain a stable skeleton structure. The H_2 consumption of Cu species in the fresh and aged catalysts is shown in Table 3, the content of isolated Cu^{II} ions in the F−NO_3 and A−NO_3 samples are much higher than the $Cu^{II}Cl_2$ and $Cu^{II}SO_4$ samples. Due to the destruction of the skeleton structure of the A−SO_4 sample, the amount of Cu^{I} is significantly reduced. During the NH_3−SCR reaction, the catalytic performance of the Cu^{II}−SSZ−13 catalysts is determined by the reducibility of active metal species in molecular sieves. Many researchers have shown that isolated Cu^{II} ion is the main active component [35,36]. Hence, the conversion of Cu^{II}−SSZ−13 catalysts will be decreased when the account of isolated Cu^{II} ion is lower. Due to the difference of copper precursors,

anions may affect the distribution of copper species in the samples. The Pauling radium increased in the order of NO_3^- (1.79 Å) ≈Cl^- (1.80 Å) < SO_4^{2-} (2.30 Å) [23]. Larger anions from the copper precursors can inhibit the entering of copper ions into the SSZ−13 pore during the formation of the colloidal process. However, the copper ions from the precursors with small anions ions like NO_3^- are more accessible to enter the pore, which generates more isolated Cu^{II}, and exhibits excellent NH_3−SCR activity.

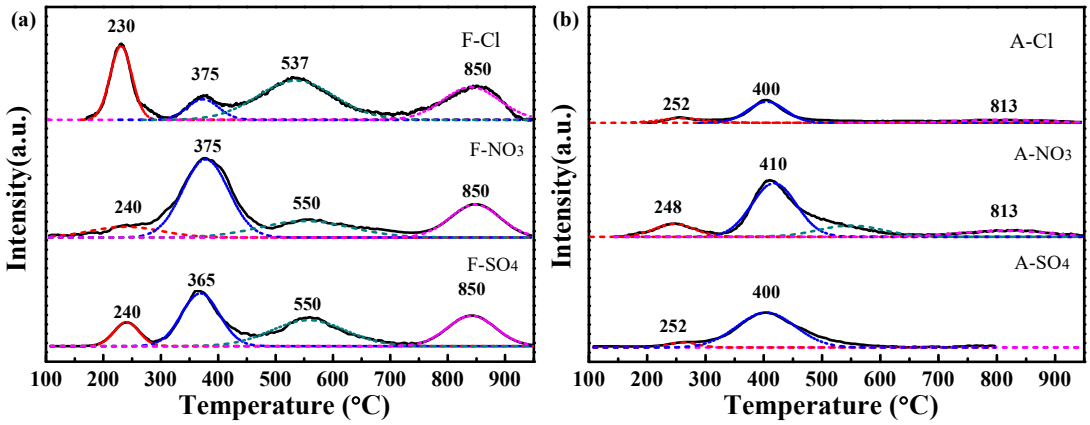

Figure 3. Hydrogen-temperature-programmed reduction (H_2-TPR) profiles of Cu^{II}−SSZ−13 catalysts before (**a**) and after (**b**) hydrothermal aging treatment.

Table 3. H_2 consumption of Cu^{II}−SSZ−13 catalysts before and after hydrothermal aging treatment.

Samples	H_2 Consumption (μmol g^{-1})				Total H_2 Consumption (μmol g^{-1})
	Cu^{II}→Cu^{I} (CHA Cages)	Cu^{II}→Cu^{I} (D6R)	Cu^{II}→Cu^{I} (Total)	Cu^{I}→Cu^{0}	
F−Cl	53.69	28.71	82.40	163.34	245.74
A−Cl	4.32	25.56	29.88	32.89	62.77
F−NO_3	34.75	136.46	171.21	152.76	323.97
A−NO_3	25.74	111.43	137.17	79.50	216.67
F−SO_4	28.61	87.35	115.96	133.87	249.83
A−SO_4	4.17	58.48	62.65	0	62.65

2.2.5. Ammonia Temperature-Programmed Desorption (NH_3−TPD) Results

The acid sites of the molecular sieve catalyst are beneficial to adsorption and activation of NH_3, which is one of the key steps for the reduction of NO by NH_3 molecules [2,37]. The ammonia temperature-programmed desorption (NH_3−TPD) spectra of the Cu^{II}−SSZ−13 catalysts are shown in Figure 4. The peak at 130 °C (Peak A) and 168 °C (Peak B) are attributed to the physical adsorption and weakly adsorbed NH_3 on the weak Lewis acid sites, respectively [38,39]. The peaks at 258 °C (Peak C) and above 420 °C (Peak D) belong to NH_3 adsorbed on strong Lewis acid sites originating from the isolated Cu^{II} ions and NH_3 adsorbed on Brønsted acid sites, respectively. Table 4 shows the adsorption amounts of NH_3 on the fresh and aged samples by deconvolution of the NH_3−TPD curves. The total acid amounts of all fresh samples are similar. Additionally, the adsorption amount of ammonia decreases and the ammonia oxidation reaction has occurred during temperature increase, causing the activity of the catalyst to decrease. After hydrothermal aging, the NH_3 adsorption peaks all decreased due to the destruction of the CHA structure and the loss of the isolated Cu^{II} ions, which is demonstrated by the results of H_2−TPR and XRD characterization. Many studies have shown that the chemisorption of NH_3 plays a significant role in the NH_3−SCR performance [2,30,40].

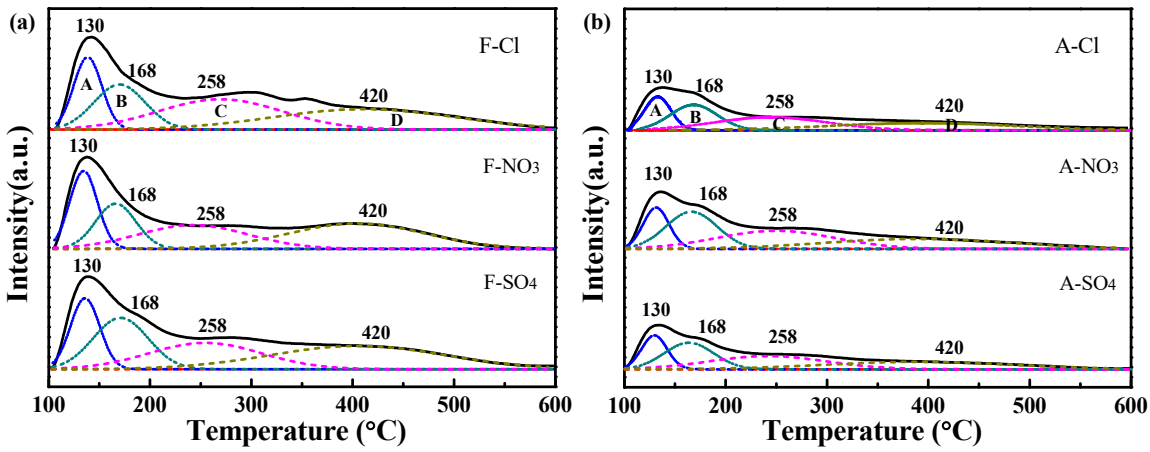

Figure 4. Ammonia temperature-programmed desorption (NH_3–TPD) profiles of Cu^{II}–SSZ–13 catalysts before (**a**) and after (**b**) hydrothermal aging treatment.

Table 4. The adsorbed NH_3 amount of Cu^{II}–SSZ–13 catalysts before and after hydrothermal aging treatment.

Samples	Adsorbed NH_3 Amount (mmol g^{-1})				Total Amount (mmol g^{-1})
	Physical Adsorption	Weak Lewis Acid Sites	Strong Lewis Acid Sites	Brønsted Acid Sites	
F–Cl	0.18	0.23	0.33	0.45	1.19
A–Cl	0.08	0.10	0.17	0.21	0.56
F–NO_3	0.20	0.21	0.32	0.54	1.27
A–NO_3	0.14	0.19	0.21	0.28	0.82
F–SO_4	0.18	0.23	0.31	0.47	1.19
A–SO_4	0.09	0.11	0.16	0.23	0.59

2.2.6. X-ray Photoelectron Spectroscopy (XPS) Results

The Cu^{II}–SSZ–13 catalysts are analyzed by Cu_{2p} X–ray photoelectron spectroscopy (XPS) in Figure 5. The fresh and aged samples have a main peak and a satellite peak of Cu $2p_{3/2}$ (930–939 and 940–948 eV) and Cu $2p_{1/2}$ (950–955 and 960.0–968 eV). The Cu $2p_{3/2}$ peaks at 935.9 eV are attributed to the isolated Cu^{II} species. The characteristic peak at 933.2 eV is ascribed to the Cu^{I} species [41,42].

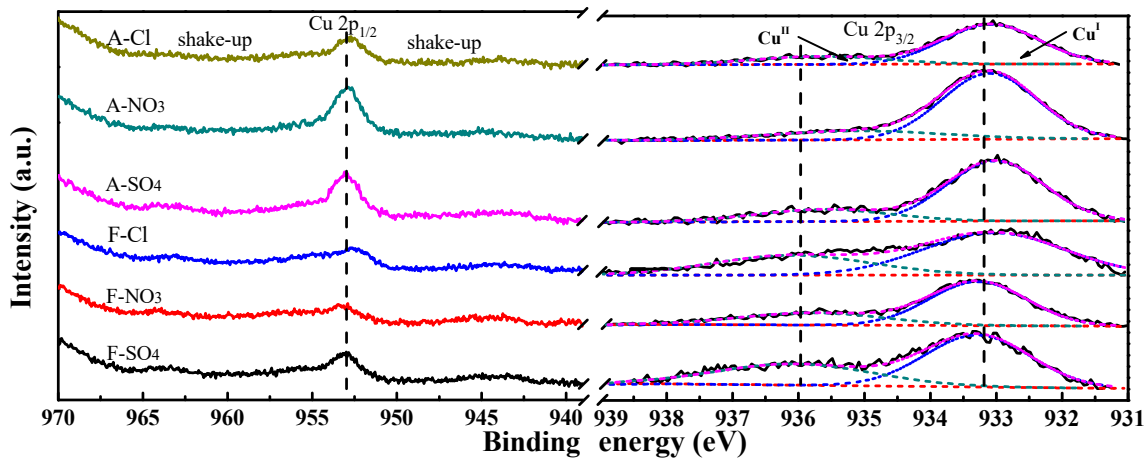

Figure 5. Cu 2p XPS spectra of Cu^{II}–SSZ–13 catalysts before and after hydrothermal aging treatment.

The Cu^{II}/Cu_{sur} ratios of all fresh sample are reduced after aging as shown in Table 5. The isolated Cu^{II} species facilitate the reduction of NO_x at low temperature, which trigger the decrease of catalytic

activity of the aged samples [37]. The Cu and Al contents of the A−SO_4 sample increase significantly and can be due to the serious destruction of the framework. However, the Cu and Al contents of A−Cl sample decrease obviously. According to the results of the ^{27}Al Nuclear Magnetic Resonance (NMR) spectra, the signal invisible of octahedral aluminum ions in the fresh and aged catalysts prepared by $Cu^{II}Cl_2$ is because that paramagnetic Cu ions may interact more strongly with the forming octahedral aluminum, which cause the decrease of surface Cu and Al species [10,43]. Furthermore, the change in XPS curve of $Cu^{II}(NO_3)_2$ sample is the least before and after aging. The Si/Al decreases slightly on the surface after aging, which may be due to aging inducing slight de-alumination. Therefore, a small portion of aluminum migrates to the surface, which maintains good anti-aging properties of the skeleton structure.

Table 5. Cu $2p_{3/2}$ XPS curve-fitting results of Cu^{II}−SSZ−13 catalysts before and after hydrothermal aging treatment.

Samples	Cu_{sur} (wt%)	Cu^{II}/Cu_{sur}	Cu^{II}/Cu^{I}	Si_{sur} (wt%)	Al_{sur} (wt%)	Si/Al_{sur}
F−Cl	0.56	0.44	0.63	6.59	3.42	1.93
A−Cl	0.29	0.15	0.35	6.30	2.66	2.37
F−NO_3	0.34	0.30	0.61	6.36	2.44	2.61
A−NO_3	0.57	0.17	0.39	6.66	2.95	2.26
F−SO_4	0.26	0.38	0.52	6.94	2.50	2.78
A−SO_4	0.77	0.24	0.35	6.65	3.36	1.98

2.2.7. NMR Results

In order to further study the effects of different copper precursors on the chemical environment of Si and Al in Cu^{II}−SSZ−13 catalysts, and the effect of hydrothermal aging treatment, ^{29}Si NMR and ^{27}Al NMR were performed for the fresh and aged catalysts. It can be seen from the ^{27}Al NMR spectra of Figure 6a–c that fresh samples show significant Al^{3+} tetrahedral coordination framework features that appear at ~58.7 ppm [10,11]. The F−SO_4 and F−NO_3 show one relatively small new resonance peak at ~−1.3 ppm, which come down the extra-framework Al in octahedral [44]. It is worth noting that hydrothermal aging at 800 °C for 20 h can result in some tetrahedral aluminum transferred into penta-coordinated extra-framework aluminum structure. The resonance peak at −1.3 ppm almost disappears. Note also that the portion of Al detached from the molecular sieve framework does not appear at ~−1.3 ppm. This portion of Al stays adjacent to paramagnetic Cu sites and thus invisible to NMR [43,45]. To better compare the changes of the Al coordination structure before and after the hydrothermal aging treatment, the tetrahedral Al signal area of the fresh sample is taken as a unity. The amount of framework Al in the aged sample is normalized to reveal the dealumination during the hydrothermal treatment. The proportion of tetrahedral Al in A−Cl sample is 0.74 indicating evident dealumination. In addition, the A−SO_4 sample has the strongest pentacoordinated extra-framework aluminum structure resonance peak. The proportion of tetrahedral Al is 0.85. However, the resonance peak intensity of Al^{3+} tetrahedral coordination structure of the A-Nit. sample at 58.7 ppm is sharper. The proportion of tetrahedral Al in A−NO_3 sample is 0.94, which means that the hydrothermal aging process causes little damage to the $Cu^{II}(NO_3)_2$ sample skeleton structure. It is consistent with the results of XRD. The $Cu^{II}(NO_3)_2$ sample exhibits slight skeleton dealumination and maintains stable SSZ−13 framework structure. It is further confirmed that the $Cu^{II}(NO_3)_2$ sample has better resistance to hydrothermal aging.

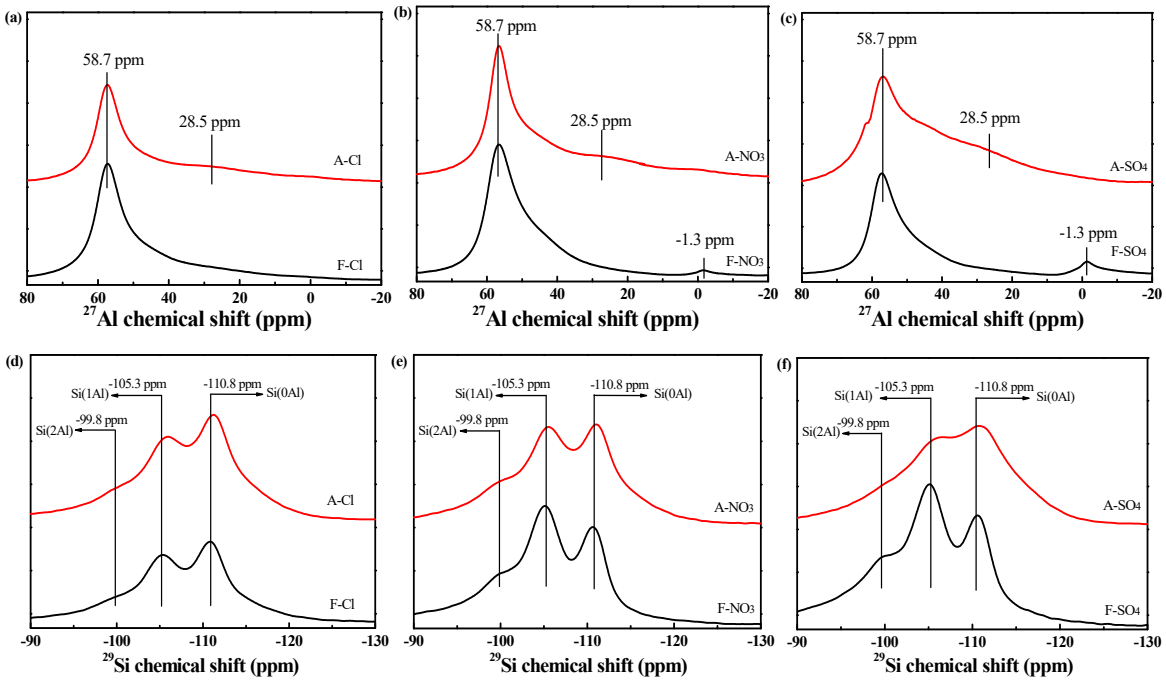

Figure 6. Solid state ^{27}Al-Nuclear Magnetic Resonance (NMR) (**a**–**c**) and ^{29}Si-NMR (**d**–**f**) spectra of Cu^{II}–SSZ–13 catalysts before and after hydrothermal aging treatment.

As seen in Figure 6d–f, wide ^{29}Si-NMR peaks with maxima at −99.8, −105.3, and −110.8 ppm are registered for Cu^{II}–SSZ–13 catalysts. These peaks are related to the following types: the structure of Si(2Al), the Si(1Al), and Si(0Al) [46,47]. The F–NO_3 sample contains more Si (2Al) and Si (2Al) and Si (1Al) structures. After aging, the peak at −105.3 ppm of three samples is weakened. The Si(1Al) structure of A–SO_4 is severely damaged, and the F–Cl sample contains more Si (0Al) structure. However, two peaks at 105.3 and 110.8 ppm become similar shoulder peaks for the A–Nit sample. Si(1Al) and Si (0Al) structures occupy a larger proportion. The catalytic properties of molecular sieves are mainly depending on the skeleton structure and surface acidity. The Si coordination structures have a significant effect on the acid intensity, which is enhanced in the order of Si(0Al) < Si(4Al) < Si(3Al) < Si(2Al) < Si(1Al) [4,27,48]. It is consistent with the results of NH_3–TPD.

3. Materials and Methods

3.1. Catalyst Preparation

The Cu^{II}–SSZ–13 catalysts were prepared by in-situ hydrothermal synthesis method using three kinds of copper precursors ($Cu^{II}(NO_3)_2$, $Cu^{II}SO_4$, $Cu^{II}Cl_2$). The copper complex (Cu–TEPA) was used as the template. An appropriate amount of silica sol (30.4%), sodium metaaluminate (99%), sodium hydroxide (96%), tetraethylenepentamine (TEPA, 95%), and deionized water, were mixed at the molar ratios of $2.5Al_2O_3$:$2.5Na_2O$:$7.4SiO_2$:$147.7H_2O$:1.47Cu–TEPA [49,50]. The formed gel was successively transferred into three 100 mL PTFE (polytetrafluoroethylene) autoclaves and crystallized at 140 °C for 72 h. The products were washed by deionized water, and dried at 100 °C for 12 h. Then, the samples was treated by ion exchange with a certain amount of NH_4NO_3 (1 mol/L) solution for 12 h at 80 °C. Finally, the samples were calcined at 550 °C for 8 h. The obtained Cu^{II}–SSZ–13 catalyst using $Cu^{II}Cl_2$, $Cu^{II}(NO_3)_2$, and $Cu^{II}SO_4$ solution as precursor were labeled as F–Cl, F–NO_3, and F–SO_4, respectively.

3.2. Hydrothermal Aging Treatment of Catalysts

To investigate the hydrothermal stability of the prepared Cu^{II}−SSZ−13 catalysts, they were aged in a fixed bed reactor containing 10 vol% H_2O under Ar atmosphere at 800 °C for 20 h. The aged catalysts were labeled as A−Cl, A−NO_3, and A−SO_4, respectively.

3.3. Catalyst Activity Evaluation

The catalytic activity was evaluated using a temperature-programmed fixed bed reactor at a gaseous hourly space velocity (GHSV) of 40,000 h^{-1}. As shown in Figure S2, the gaseous hourly space velocity (GHSV) of 40,000 h^{-1} is preferentially used as the optimal space velocity for the F−NO_3 sample. The reactor contained 0.05% NO, 0.05% NH_3, 5 vol% O_2, and 10 vol% H_2O. He was used as balance gas. The total flow rate 400 mL min^{-1}. The concentrations of NO, NH_3, N_2O, and NO_2 gases were measured in situ by a NICOLET IS10 FTIR spectrometer. The NO conversion and the N_2 selectivity were calculated based on the following equation:

$$X_{NO} = \frac{C_{NO,\ in} - C_{NO,\ out}}{C_{NO,\ out}} \times 100\%,$$

$$S_{N_2} = \left(1 - \frac{2C_{N_2O,\ out} + C_{NO_2,\ out}}{C_{NO,in} + C_{NH_3,\ in} - C_{NO,out} - C_{NH_3,\ out}}\right) \times 100\%.$$

3.4. Catalyst Characterization

The XRD analysis was carried out on a DX−2700 diffractometer (Dangdong, Dandong Aolong Ray Instrument Group Co., Ltd. China) with Cu Kα radiation (λ = 1.54184 nm) at 40 kV and 30 mA. The dates were collected with a scanning speed of 8°·min^{-1} that ranged from 5° to 60°. The SEM images of samples were obtained via a Japanese Jeol JSM-7001F instrument (JEOL, Japan) at 10 kV. H_2−TPR and NH_3−TPD experiments were carried out on the Autochem II 2920 instrument (Micromeritics, Norcross, GA, USA). For H_2−TPR measurement, 100 mg of sample was set into a quartz reactor and pretreated at 300 °C for 0.5 h in Ar atmosphere. After cooling to room temperature (25 °C), the gas was switched to a 10 vol% H_2−Ar mixture gas with the temperature increased from 50 to 1000 °C at a rate of 10 °C min^{-1}. For NH_3−TPD measurement, the pretreatment was as same as the H_2−TPR process and then exposed to 10% NH_3/He at 50 °C for 30 min, followed by a temperature ramp to 600 °C at a rate of 10 °C min^{-1}. The pore structure analysis of the samples was acquired on a JW-BK122W N_2 adsorption-desorption instrument (Beijing, JWGB Sci. & Tech. Co., Ltd., China) by using liquid nitrogen at 77 K (−196 °C). XPS measurements were performed on an AXIS ULTRA DLD electron spectrometer (Kratos corporation, UK) with a monochromatic Al Kα (hv = 1486.6 eV) as excitation source. ^{27}Al and ^{29}Si solid state NMR spectra were collected by an Avance III 600 MHz instrument (Bruker, UK). ^{29}Si MAS NMR spectra were recorded at a rate of 5 kHz and 7 mm probe. ^{27}Al MAS NMR spectra were recorded at a rate of 13 kHz using a 4 mm probe.

4. Conclusions

In summary, the Cu^{II}−SSZ−13 catalysts were prepared by in-situ hydrothermal synthesis method using various copper precursors ($Cu^{II}(NO_3)_2$, $Cu^{II}SO_4$, $Cu^{II}Cl_2$) for NO selective catalytic reduction with NH_3 in simulated diesel vehicle exhausts. The $Cu^{II}(NO_3)_2$ sample not only exhibits outstanding catalytic activity and N_2 selectivity, but also has higher anti-aging properties. The F−NO_3 sample exceeded 90% conversion at a wide range of 180~700 °C. After aging for 20 h at 800 °C, the A−NO_3 sample still exhibits above 90% NO conversion in the temperature range of 240–600 °C. The difference of deNO_x activity and anti-aging performance can be tuned by copper precursor due to the anion's effect. The Pauling radium of the anion affects the distribution of copper species in the Cu^{II}-SSZ-13 catalyst. The larger anions could impede the entry of copper ions into the pores and gathered on the out surface of the molecular sieve. In addition, the adsorption capacity of different anions to

the cations will affect the nucleation, and the growth process of SSZ−13 can affect the crystallization process. More isolated Cu^{II} ions are adsorbed in the framework of the Cu^{II}−SSZ−13 catalyst and served as active sites for the NH_3−SCR reaction resulting in excellent catalytic activity. Furthermore, after hydrothermal aging treatment, the $Cu^{II}(NO_3)_2$ sample remains stable in the SSZ-13 framework resulting in maintaining its high catalytic activity. Our work can help to understand the effect of anions originating from copper precursors on the structure and catalytic property and rational design of a Cu^{II}−SSZ−13 catalyst for NO selective catalytic reduction with NH_3 in diesel vehicle exhausts.

Supplementary Materials: The following are available online at http://www.mdpi.com/2073-4344/9/9/781/s1, Figure S1: XRD patterns of Cu^{II}−SSZ−13 catalysts before (a) and after (b) hydrothermal aging treatment. Figure S2: Gaseous hourly space velocity (GHSV) of fresh Cu^{II}−SSZ−13 catalyst synthesized by $Cu^{II}(NO_3)_2$ as copper precursors.

Author Contributions: The experimental work was conceived and designed by M.W. and J.W.; M.W. and Z.P. performed the experiments; M.W. and M.L. analyzed the data and M.W. drafted the paper. The manuscript was amended through the comments of C.Z., W.B., L.C., L.H., Y.H., Z.H. and. All authors have given approval for the final version of the manuscript.

Funding: The authors gratefully thank the Project funded by China Postdoctoral Science Foundation (2019M651077).

Conflicts of Interest: The authors declare no conflict of interest.

References

1. Liu, F.; Yu, Y.; He, H. Environmentally-benign catalysts for the selective catalytic reduction of NO_x from diesel engines: Structure–activity relationship and reaction mechanism aspects. *Chem. Commun.* **2014**, *50*, 8445–8463. [CrossRef] [PubMed]
2. Han, S.; Ye, Q.; Cheng, S.; Kang, T.; Dai, H. Effect of the hydrothermal aging temperature and Cu/Al ratio on the hydrothermal stability of CuSSZ-13 catalysts for NH_3-SCR. *Catal. Sci. Technol.* **2017**, *7*, 703–717. [CrossRef]
3. Xin, Y.; Li, Q.; Zhang, Z. Zeolitic materials for $DeNO_x$ selective catalytic reduction. *ChemCatChem* **2018**, *10*, 29–41. [CrossRef]
4. Wang, J.; Peng, Z.; Chen, Y.; Bao, W.; Chang, L.; Feng, G. In-situ hydrothermal synthesis of Cu-SSZ-13/cordierite for the catalytic removal of NO_x from diesel vehicles by NH_3. *Chem. Eng. J.* **2015**, *263*, 9–19. [CrossRef]
5. Kwon, D.W.; Nam, K.B.; Hong, S.C. The role of ceria on the activity and SO_2 resistance of catalysts for the selective catalytic reduction of NO_x by NH_3. *Appl. Catal. B* **2015**, *166*, 37–44. [CrossRef]
6. He, Y.; Ford, M.E.; Zhu, M.; Liu, Q.; Tumuluri, U.; Wu, Z.; Wachs, I.E. Influence of catalyst synthesis method on selective catalytic reduction (SCR) of no by NH_3 with V_2O_5-WO_3/TiO_2 catalysts. *Appl. Catal. B* **2016**, *193*, 141–150. [CrossRef]
7. Joshi, S.Y.; Kumar, A.; Luo, J.; Kamasamudram, K.; Currier, N.W.; Yezerets, A. New insights into the mechanism of NH_3-SCR over Cu- and Fe-zeolite catalyst: Apparent negative activation energy at high temperature and catalyst unit design consequences. *Appl. Catal. B* **2018**, *226*, 565–574. [CrossRef]
8. Xie, K.; Woo, J.; Bernin, D.; Kumar, A.; Kamasamudram, K.; Olsson, L. Insights into hydrothermal aging of phosphorus-poisoned Cu-SSZ-13 for NH_3-SCR. *Appl. Catal. B* **2019**, *241*, 205–216. [CrossRef]
9. Cheng, J.; Han, S.; Ye, Q.; Cheng, S.; Kang, T.; Dai, H. Selective catalytic reduction of NO with NH_3 over the Cu/SAPO-34 catalysts derived from different Cu precursors. *Microporous Mesoporous Mater.* **2019**, *278*, 423–434. [CrossRef]
10. Kwak, J.H.; Tran, D.; Burton, S.D.; Szanyi, J.; Lee, J.H.; Peden, C.H.F. Effects of hydrothermal aging on NH_3-SCR reaction over Cu/zeolites. *J. Catal.* **2012**, *287*, 203–209. [CrossRef]
11. Han, L.; Zhao, X.; Yu, H.; Hu, Y.; Li, D.; Sun, D.; Liu, M.; Chang, L.; Bao, W.; Wang, J. Preparation of SSZ-13 zeolites and their NH_3-selective catalytic reduction activity. *Microporous Mesoporous Mater.* **2018**, *261*, 126–136. [CrossRef]
12. Shishkin, A.; Kannisto, H.; Carlsson, P.-A.; Härelind, H.; Skoglundh, M. Synthesis and functionalization of SSZ-13 as an NH_3-SCR catalyst. *Catal. Sci. Technol.* **2014**, *4*, 3917–3926. [CrossRef]

13. Ren, L.; Zhu, L.; Yang, C.; Chen, Y.; Sun, Q.; Zhang, H.; Li, C.; Nawaz, F.; Meng, X.; Xiao, F.S. Designed copper-amine complex as an efficient template for one-pot synthesis of Cu-SSZ-13 zeolite with excellent activity for selective catalytic reduction of NO_x by NH_3. *Chem. Commun.* **2011**, *47*, 9789–9791. [CrossRef] [PubMed]
14. Zhang, T.; Qiu, F.; Chang, H.; Li, X.; Li, J. Identification of active sites and reaction mechanism on low-temperature SCR activity over Cu-SSZ-13 catalysts prepared by different methods. *Catal. Sci. Technol.* **2016**, *6*, 6294–6304. [CrossRef]
15. Ma, Y.; Cheng, S.; Wu, X.; Shi, Y.; Cao, L.; Liu, L.; Ran, R.; Si, Z.; Liu, J.; Weng, D. Low-temperature solid-state ion-exchange method for preparing Cu-SSZ-13 selective catalytic reduction catalyst. *ACS Catal.* **2019**, *9*, 6962–6973. [CrossRef]
16. Paolucci, C.; Khurana, I.; Parekh, A.A.; Li, S.; Shih, A.J.; Li, H.; di Iorio, J.R.; Albarracin-Caballero, J.D.; Yezerets, A.; Miller, J.T.; et al. Dynamic multinuclear sites formed by mobilized copper ions in NO_x selective catalytic reduction. *Science* **2017**, *357*, 898–903. [CrossRef]
17. Borfecchia, E.; Beato, P.; Svelle, S.; Olsbye, U.; Lamberti, C.; Bordiga, S. Cu-cha—A model system for applied selective redox catalysis. *Chem. Soc. Rev.* **2018**, *47*, 8097–8133. [CrossRef] [PubMed]
18. Marberger, A.; Petrov, A.W.; Steiger, P.; Elsener, M.; Kröcher, O.; Nachtegaal, M.; Ferri, D. Time-resolved copper speciation during selective catalytic reduction of no on Cu-SSZ-13. *Nat. Catal.* **2018**, *1*, 221–227. [CrossRef]
19. Xu, R.; Pang, W.; Yu, J.; Huo, Q.; Chen, J. *Molecular Sieves and Porous Materials Chemietry*; Science Press: Beijing, China, 2004.
20. Kumar, R.; Mukherjee, P.; Pandey, R.K.; Rajmohanan, P.; Bhaumik, A. Role of oxyanions as promoter for enhancing nucleation and crystallization in the synthesis of MFI-type microporous materials. *Microporous Mesoporous Mater.* **1998**, *22*, 23–31. [CrossRef]
21. López-León, T.; Santander-Ortega, M.J.; Ortega-Vinuesa, J.L.; Bastos-González, D. Hofmeister Effects in Colloidal Systems: Influence of the Surface Nature. *J. Phys. Chem. C* **2008**, *112*, 16060–16069. [CrossRef]
22. Toktarev, A.V.; Echevskii, G.V. Hofmeister anion effect on the formation of zeolite beta. *Stud. Surf. Sci. Catal.* **2008**, *174*, 167–172.
23. Leontidis, E. Hofmeister anion effects on surfactant self-assembly and the formation of mesoporous solids. *Curr. Opin. Colloid Interface Sci.* **2002**, *7*, 81–91. [CrossRef]
24. Yang, Z. Hofmeister effects: An explanation for the impact of ionic liquids on biocatalysis. *J. Biotechnol.* **2009**, *144*, 12–22. [CrossRef] [PubMed]
25. Gao, F.; Walter, E.D.; Kollar, M.; Wang, Y.; Szanyi, J.; Peden, C.H.F. Understanding ammonia selective catalytic reduction kinetics over Cu/SSZ-13 from motion of the Cu ions. *J. Catal.* **2014**, *319*, 1–14. [CrossRef]
26. Ma, L.; Cheng, Y.; Cavataio, G.; McCabe, R.W.; Fu, L.; Li, J. Characterization of commercial Cu-SSZ-13 and Cu-SAPO-34 catalysts with hydrothermal treatment forNH_3-SCR of NO_x in diesel exhaust. *Chem. Eng. J.* **2013**, *225*, 323–330. [CrossRef]
27. Kwak, J.H.; Tonkyn, R.G.; Kim, D.H.; Szanyi, J.; Peden, C.H.F. Excellent activity and selectivity of Cu-SSZ-13 in the selective catalytic reduction of NO_x with NH_3. *J. Catal.* **2010**, *275*, 187–190. [CrossRef]
28. Zhu, H.; Kwak, J.H.; Peden, C.H.F.; Szanyi, J. In situ DRIFTS-MS studies on the oxidation of adsorbed NH_3 by NO_x over a Cu-SSZ-13 zeolite. *Catal. Today* **2013**, *205*, 16–23. [CrossRef]
29. Wang, J.; Peng, Z.; Qiao, H.; Yu, H.; Hu, Y.; Chang, L.; Bao, W. Cerium-Stabilized Cu-SSZ-13 Catalyst for the Catalytic Removal of NO_x by NH_3. *Ind. Eng. Chem. Res.* **2016**, *55*, 1174–1182. [CrossRef]
30. Fan, C.; Chen, Z.; Pang, L.; Ming, S.; Dong, C.; Brou Albert, K.; Liu, P.; Wang, J.; Zhu, D.; Chen, H.; et al. Steam and alkali resistant Cu-SSZ-13 catalyst for the selective catalytic reduction of NO_x in diesel exhaust. *Chem. Eng. J.* **2018**, *334*, 344–354. [CrossRef]
31. Xie, L.; Liu, F.; Ren, L.; Shi, X.; Xiao, F.S.; He, H. Excellent performance of one-pot synthesized Cu-SSZ-13 catalyst for the selective catalytic reduction of NO_x with NH_3. *Environ. Sci. Technol.* **2014**, *48*, 566–572. [CrossRef]
32. Zhang, T.; Qiu, F.; Li, J. Design and synthesis of core-shell structured meso-Cu-SSZ-13@mesoporous aluminosilicate catalyst for SCR of NO_x with NH_3: Enhancement of activity, hydrothermal stability and propene poisoning resistance. *Appl. Catal. B* **2016**, *195*, 48–58. [CrossRef]

33. Xu, M.; Wang, J.; Yu, T.; Wang, J.; Shen, M. New insight into Cu/SAPO-34 preparation procedure: Impact of NH_4-SAPO-34 on the structure and Cu distribution in Cu-SAPO-34 NH_3-SCR catalysts. *Appl. Catal. B* **2018**, *220*, 161–170. [CrossRef]
34. Chen, Z.; Fan, C.; Pang, L.; Ming, S.; Liu, P.; Li, T. The influence of phosphorus on the catalytic properties, durability, sulfur resistance and kinetics of Cu-SSZ-13 for NO_x reduction by NH_3-SCR. *Appl. Catal. B* **2018**, *237*, 116–127. [CrossRef]
35. Fickel, D.W.; Lobo, R.F. Coordination in Cu-SSZ-13 and Cu-SSZ-16 Investigated by Variable-Temperature XRD. *J. Phys. Chem. C* **2009**, *114*, 1633–1640. [CrossRef]
36. Deka, U.; Juhin, A.; Eilertsen, E.A.; Emerich, H.; Green, M.A.; Korhonen, S.T.; Weckhuysen, B.M.; Beale, A.M. Confirmation of Isolated Cu^{2+} Ions in SSZ-13 Zeolite as Active Sites in NH_3-Selective Catalytic Reduction. *J. Phys. Chem. C* **2012**, *116*, 4809–4818. [CrossRef]
37. Chen, J.; Zhao, R.; Zhou, R. A new insight into active Cu^{2+} Species Properties in One-Pot Synthesized Cu-SSZ-13 Catalysts for NO_x Reduction by NH_3. *ChemCatChem* **2018**, *10*, 5182–5189. [CrossRef]
38. Gao, F.; Washton, N.M.; Wang, Y.; Kollár, M.; Szanyi, J.; Peden, C.H.F. Effects of Si/Al ratio on Cu/SSZ-13 NH_3-SCR catalysts: Implications for the active Cu species and the roles of Brønsted acidity. *J. Catal.* **2015**, *331*, 25–38. [CrossRef]
39. Gao, F.; Wang, Y.; Washton, N.M.; Kollár, M.; Szanyi, J.; Peden, C.H.F. Alkali and Alkaline Earth Cocations on the Activity and Hydrothermal Stability of Cu/SSZ-13 NH_3–SCR Catalysts. *ACS Catal.* **2015**, *5*, 6780–6791. [CrossRef]
40. Lezcano-Gonzalez, I.; Deka, U.; van der Bij, H.E.; Paalanen, P.; Arstad, B.; Weckhuysen, B.M.; Beale, A.M. Chemical deactivation of Cu-SSZ-13 ammonia selective catalytic reduction (NH_3-SCR) systems. *Appl. Catal. B* **2014**, *154*, 339–349. [CrossRef]
41. Wang, J.; Liu, Z.; Feng, G.; Chang, L.; Bao, W. In situ synthesis of CuSAPO-34/cordierite and its selective catalytic reduction of nitrogen oxides in vehicle exhaust: The effect of HF. *Fuel* **2013**, *109*, 101–109. [CrossRef]
42. Chen, B.; Xu, R.; Zhang, R.; Liu, N. Economical Way to Synthesize SSZ-13 with abundant ion-exchanged Cu^+ for an extraordinary performance in selective catalytic reduction (SCR) of NO_x by ammonia. *Environ. Sci. Technol.* **2014**, *48*, 13909–13916. [CrossRef] [PubMed]
43. Song, J.; Wang, Y.; Walter, E.D.; Washton, N.M.; Mei, D.; Kovarik, L.; Engelhard, M.H.; Prodinger, S.; Wang, Y.; Peden, C.H.F.; et al. Toward rational design of Cu/SSZ-13 selective catalytic reduction catalysts: Implications from atomic-level understanding of hydrothermal stability. *ACS Catal.* **2017**, *7*, 8214–8227. [CrossRef]
44. Wu, L.; Degirmenci, V.; Magusin, P.C.M.M.; Lousberg, N.J.H.G.M.; Hensen, E.J.M. Mesoporous SSZ-13 zeolite prepared by a dual-template method with improved performance in the methanol-to-olefins reaction. *J. Catal.* **2013**, *298*, 27–40. [CrossRef]
45. Prodinger, S.; Derewinski, M.A.; Wang, Y.; Washton, N.M.; Walter, E.D.; Szanyi, J.; Gao, F.; Wang, Y.; Peden, C.H.F. Sub-micron Cu/SSZ-13: Synthesis and application as selective catalytic reduction (SCR) catalysts. *Appl. Catal. B* **2017**, *201*, 461–469. [CrossRef]
46. Martins, G.A.V.; Berlier, G.; Coluccia, S.; Pastore, H.O.; Superti, G.B.; Gatti, G.; Marchese, L. Revisiting the nature of the acidity in chabazite-related Silicoaluminophosphates: Combined FTIR and ^{29}Si MAS NMR study. *J. Phys. Chem. C* **2007**, *111*, 330–339. [CrossRef]
47. Xu, L.; Du, A.; Wei, Y.; Wang, Y.; Yu, Z.; He, Y.; Zhang, X.; Liu, Z. Synthesis of SAPO-34 with only Si(4Al) species: Effect of Si contents on Si incorporation mechanism and Si coordination environment of SAPO-34. *Microporous and Mesoporous Mater.* **2008**, *115*, 332–337. [CrossRef]
48. Barthomeuf, D. Topological model for the compared acidity of SAPOs and SiAl zeolites. *Zeolites* **1994**, *14*, 394–401. [CrossRef]

49. Ren, L.; Zhang, Y.; Zeng, S.; Zhu, L.; Sun, Q.; Zhang, H.; Yang, C.; Meng, X.; Yang, X.; Xiao, F.-S. Design and synthesis of a catalytically active Cu-SSZ-13 zeolite from a copper-amine complex template. *Chin. J. Catal.* **2012**, *33*, 92–105. [CrossRef]
50. Wang, J.; Peng, Z.; Qiao, H.; Han, L.; Bao, W.; Chang, L.; Feng, G.; Liu, W. Influence of aging on in situ hydrothermally synthesized Cu-SSZ-13 catalyst for NH_3-SCR reaction. *RSC Adv.* **2014**, *4*, 42403–42411. [CrossRef]